Development 136, 1633-1641 (2009) doi:10.1242/dev.030924

Distinct phases of cardiomyocyte differentiation regulate growth of the zebrafish heart

Emma de Pater[1], Linda Clijsters[1], Sara R. Marques[2,3], Yi-Fan Lin[2], Zayra V. Garavito-Aguilar[2], Deborah Yelon[2,*] and Jeroen Bakkers[1,4,*]

Amongst animal species, there is enormous variation in the size and complexity of the heart, ranging from the simple one-chambered heart of *Ciona intestinalis* to the complex four-chambered heart of lunged animals. To address possible mechanisms for the evolutionary adaptation of heart size, we studied how growth of the simple two-chambered heart in zebrafish is regulated. Our data show that the embryonic zebrafish heart tube grows by a substantial increase in cardiomyocyte number. Augmented cardiomyocyte differentiation, as opposed to proliferation, is responsible for the observed growth. By using transgenic assays to monitor developmental timing, we visualized for the first time the dynamics of cardiomyocyte differentiation in a vertebrate embryo. Our data identify two previously unrecognized phases of cardiomyocyte differentiation separated in time, space and regulation. During the initial phase, a continuous wave of cardiomyocyte differentiation begins in the ventricle, ends in the atrium, and requires Islet1 for its completion. In the later phase, new cardiomyocytes are added to the arterial pole, and this process requires Fgf signaling. Thus, two separate processes of cardiomyocyte differentiation independently regulate growth of the zebrafish heart. Together, our data support a model in which modified regulation of these distinct phases of cardiomyocyte differentiation has been responsible for the changes in heart size and morphology among vertebrate species.

KEY WORDS: Fgf, Differentiation, Heart, Islet1, Zebrafish

INTRODUCTION

The vertebrate heart acquires its three-dimensional (3D) structure during embryonic development. In all vertebrates, the heart starts out as a simple linear tube. Expansion of the linear heart tube is followed by valve formation and septation to form a two-, three- or four-chambered heart. The regulation of heart size and its relationship to the evolution of the cardiac chambers remain long-standing mysteries.

Growth of the heart tube could be mediated either through cell proliferation or by recruitment of new cardiomyocytes into the organ. Although cardiac cells do proliferate, it is rare in the linear heart tube. In the chick heart, myocardial proliferation only starts at stage 12, when the heart tube has already looped and chambers start to emerge (Soufan et al., 2006). The early work of de la Cruz in the chick embryo demonstrated that the heart lengthens by the addition of cells to the arterial (outflow) pole of the heart (de la Cruz et al., 1977). Later studies in mouse and chick confirmed that, in these organisms, the embryonic primitive heart tube grows and becomes structurally elaborate owing to the significant addition of cells to the right ventricle and the outflow tract (OFT) from the pharyngeal mesoderm, which is also referred to as the secondary or anterior heart field (Kelly et al., 2001; Mjaatvedt et al., 2001; Waldo et al., 2001). Later studies revealed an extension of this population of progenitor cells, more posteriorly, that also contribute to the venous pole of the heart (atria) (Cai et al., 2003). The progenitor cells located within the pharyngeal mesoderm that contribute cardiomyocytes to both the arterial pole and the venous pole are referred to as the second heart field (SHF), as opposed to the first heart field, which gives rise to the cells of the early cardiac tube (Buckingham et al., 2005). A lack of markers that are specific for the primary heart field has made it difficult to determine its location. The recent observation that Islet1 protein, previously used as a marker for the SHF, is present in all cardiomyocytes has initiated a discussion about significance of the different heart fields (Prall et al., 2007). This discussion has led to the alternative suggestion that the heart tube grows by a continuous differentiation process (Moorman et al., 2007). However, the inability to visualize cardiomyocyte differentiation has made it difficult to resolve these issues.

Here, we investigate the dynamics of cardiomyocyte differentiation during cardiac development, and by taking advantage of opportunities for high-resolution and live imaging of the zebrafish heart, we visualize this process for the first time. By using a developmental timing assay and a photoconvertible marker, we identify two phases of cardiomyocyte differentiation. These previously unrecognized phases of cardiomyocyte differentiation are separated in time, space and the molecular mechanisms by which they are controlled.

MATERIALS AND METHODS

Zebrafish lines

All transgenic strains were analyzed as heterozygotes in our studies, and all embryos were grown at 28.5°C. To identify cardiomyocytes and for the developmental timing assay we used *Tg(myl7:EGFP)twu26* (Huang et al., 2003) and *Tg(–5.1myl7:nDsRed2)f2* (Mably et al., 2003) lines. Founder fish with germline integration of *Tg(cmlc2:kaede)* were generated by Tol2 transposase-mediated transgenesis (Fisher et al., 2006) and were outcrossed to produce embryos for photoconversion. The *islet1* mutant K88X (*isl1*^{SA0029}) was isolated from an ENU-mutagenized library, using target-selected mutagenesis, as described before (Wienholds et al., 2002).

[1]Hubrecht Institute and University Medical Centre Utrecht, 3584 CT, Utrecht, The Netherlands. [2]Kimmel Center for Biology and Medicine, Skirball Institute of Biomolecular Medicine, New York University School of Medicine, New York, NY 10016, USA. [3]Graduate Program in Areas of Basic and Applied Biology, Universidade do Porto, 4050-465 Porto, Portugal. [4]Interuniversity Cardiology Institute of the Netherlands, 3511 GC, Utrecht, The Netherlands.

*Authors for correspondence (e-mails: yelon@saturn.med.nyu.edu; j.bakkers@niob.knaw.nl)

Accepted 4 March 2009

Cell counts and developmental timing assay

To count cardiomyocytes at various stages, we used the *Tg(cmlc2:dsred2-nuc)* line stained using an α-DsRed antibody (Clontech). The embryos were grown under normal culture conditions (Westerfield, 1995) up to the desired stage and subsequently fixed (overnight at 4°C) in 2% paraformaldehyde containing glycerol and washed with PBS containing 0.1% Tween (PBST) the following day. The embryos were counterstained with DAPI [15 minutes at room temperature, 1:5000 DAPI (Boehringer Mannheim) in PBST]. The embryos were flat-mounted and imaged ventrally in Vectashield containing DAPI (Vector Laboratories).

Mounted embryos were imaged using a Leica TCS SPE confocal microscope with a 20× oil immersion lens. The images were zoomed in to 1.96× with the LAS-AF TCS SPE software and sequential confocal images were taken using the laser channels 405, 488 and 532 nm with a standardized step size of 0.642 μm in the *z*-direction. The pinhole was set to 1 airy unit and the scanning speed was 600 Hz.

3D reconstructions of confocal stacks were made using Volocity version 4.1 software (Improvision). Quantification of the $GFP^{pos}DsRed^{pos}$ and $GFP^{pos}DsRed^{neg}$ myocardial cells was also performed using Volocity 4.1 software. For each individual cell positive in the GFP channel, it was carefully determined whether it was $DsRed^{pos}$ or $DsRed^{neg}$ by opening and closing the different channels. All embryos were counted at least two times.

Photoconversion of Kaede

Photoconversion of Kaede fluorescence from green to red was achieved by exposing transgenic embryos to UV light on a Zeiss Axioplan microscope equipped with a DAPI filter set, as previously described (Hatta et al., 2006). Confocal *z*-stacks were obtained using a Zeiss LSM 510 laser-scanning microscope and analyzed with Zeiss LSM and Volocity software.

Histological methods

BrdU labeling was performed by soaking the embryos in embryo medium containing 5 mg/ml BrdU (Roche) for 24 hours. α-BrdU (Roche) and α-phospho-His (Upstate) antibody labeling was performed on 6- and 10-μm thick paraffin sections, respectively, which were then stained with 3,3′-Diaminobenzidine (DAB). Other antibodies used in this study were: α-DsRed (Clontech), α-eGFP (Chemokine) and α-Isl (Hybridoma bank clone 39.4D5). Immunofluorescence was performed according to Smith et al. (Smith et al., 2008).

SU5402 treatment

Embryos were treated with either DMSO or SU5402 at a concentration of 12.5 μM in embryo medium from 24 hpf until 48 hpf in glass vials in the dark at normal culture temperatures.

Morpholinos

Antisense morpholinos targeting *fgf8* (Draper et al., 2001) or *isl1* (Hutchinson and Eisen, 2006) were injected at the one-cell stage. Uninjected and control MO (Gene Tools) injected embryos from the same egg lay were used as controls for all experiments.

RESULTS

Cardiomyocyte cell number in the zebrafish heart tube increases during looping

Growth of the two-chambered zebrafish heart has not been studied systematically. To determine the number of cells in the zebrafish heart, we counted the differentiated cardiomyocytes present in the linear heart tube and the looped chambers. We used *Tg(cmlc2:dsred2-nuc2)* embryos that express nuclear DsRed from the *cardiac myosin light chain 2* (*cmlc2*; *myl7* – Zebrafish Information Network) promoter in all differentiated cardiomyocytes (Mably et al., 2003). To identify all cardiomyocytes expressing DsRed, *Tg(cmlc2:dsred2-nuc)* embryos were fixed for immunofluorescence staining using an α-DsRed antibody (Fig. 1A-F). At 24 hours post-fertilization (hpf), the heart tube has formed from the cardiac disk and was found to contain 151±12 (mean±s.e.m., *n*=5) cardiomyocytes. Over the next 24 hours, a

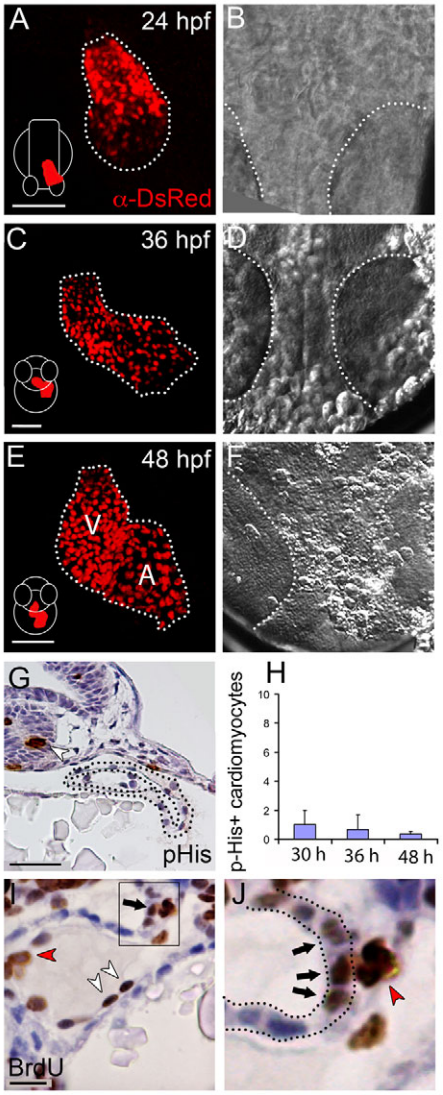

Fig. 1. Insufficient proliferation in the myocardium to account for the increase of cardiomyocyte number in the zebrafish heart. (**A**,**C**,**E**) To quantify cardiomyocyte numbers at various stages of development, *Tg(cmlc2:dsred2-nuc)* embryos of 24, 36 and 48 hpf were fixed, stained using an α-DsRed antibody and imaged by confocal microscopy. Maximum projections of the DsRed signal is shown in these panels. The dotted line outlines the heart tube; the arterial pole (outflow) is to the top and the venous pole (inflow) to the bottom. Schematics of embryos at the various developmental stages are shown in the left bottom of panels A, C and E; white outlines the embryo and red represents the forming heart tube at each stage. The 24 hpf embryo is shown in dorsal view, the 36 and 48 hpf embryos in anterior view. V, ventricle; A, atrium. (**B**,**D**,**F**) Brightfield images of the embryos shown in A, C and E; dotted lines outline the eyes. (**G**) Phospho-His staining (brown) on transverse sections through the heart at 36 hpf. The dotted line indicates the myocardium; white arrowhead indicates a phospho-His-positive cell in the neural tube. (**H**) The total number of phospho-His-positive myocardial cells/embryo at 30 (*n*=3), 36 (*n*=3) and 48 hpf (*n*=6). Bars represent mean±s.e.m. (**I**,**J**) BrdU labeling from 24-48 hpf. White arrowheads indicate BrdU-positive (brown) endocardial cells; red arrowhead indicates a BrdU-positive blood cell; black arrow indicates BrdU-positive myocardial cells. (J) Enlargement of the black box in I indicating BrdU-positive cells in the arterial pole of the 48 hpf zebrafish heart; dotted lines outline the myocardium. Scale bars: 50 μm in A,C,E; 25 μm in G; 10 μm in I.

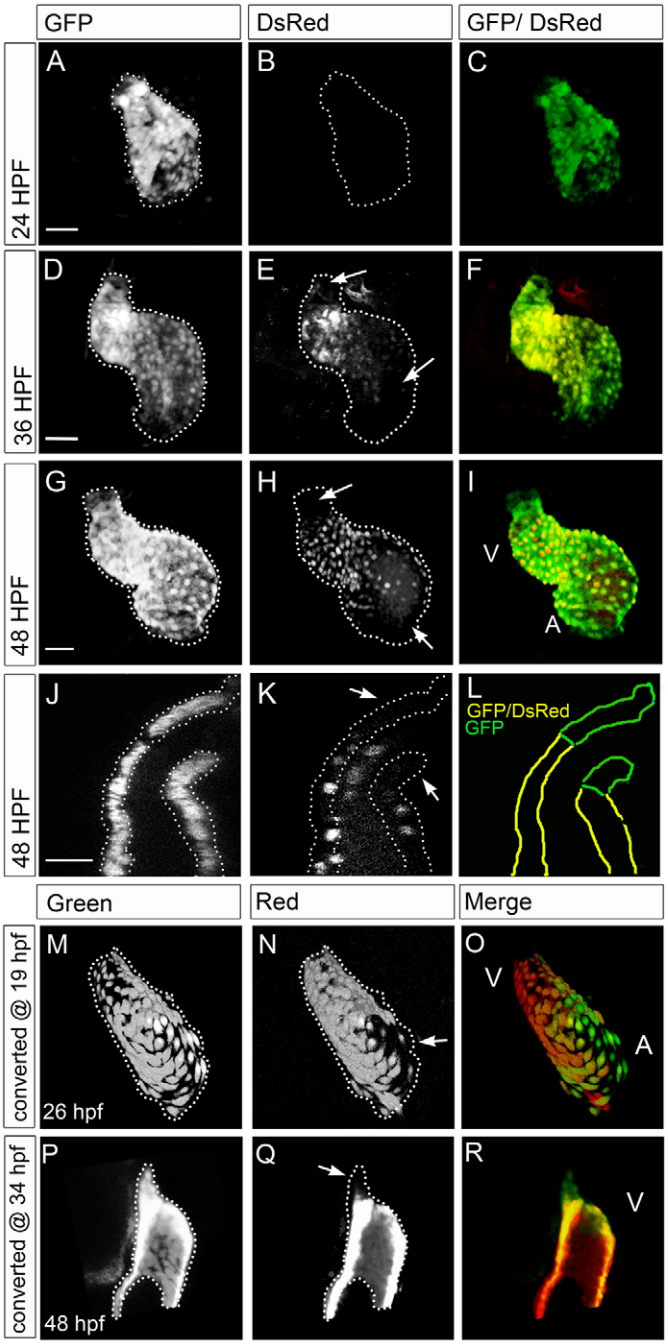

Fig. 2. Delayed cardiomyocyte differentiation first arises at the venous pole and later also contributes cells to the arterial pole. (**A-I**) Developmental timing assay images: reconstruction of confocal *z*-stacks of eGFP (A,D,G), DsRed (B,E,H), and overlay (C,F,I) from *Tg(cmlc2:eGFP)/Tg(cmlc2:dsred2-nuc)* embryos. The arterial pole is to the top left; dotted lines outline the eGFP positive heart tubes. Scale bars: 50 μm. (A-C) At 24 hpf, eGFP fluorescence was visible in the entire heart tube. At this time point, no DsRed fluorescence was observed. (D-F) At 36 hpf, the eGFP fluorescence was visible in the entire heart tube. DsRed fluorescence was detected only in the ventricle and at the inner curvature of the atrium. Arrows indicate the regions in the heart tube that are negative for the DsRed signal. (G-I) At 48 hpf, both GFP and DsRed fluorescence were observed in the heart tube. The DsRed signal remained absent from the poles (arrows), which were positive for eGFP. (**J**,**K**) Single confocal scan from *Tg(cmlc2:GFP)/Tg(cmlc2:dsred2-nuc)* embryos at 48 hpf at the level of the arterial pole. Dotted lines indicates the eGFP signal shown in J; arrows in K indicate the most distal outflow tract cells that are positive for eGFP but negative for DsRed. The signal within the heart lumen detected in K but not in J is derived from background fluorescence from red blood cells. Scale bar: 25 μm. (**L**) Schematic of the location of the $eGFP^{pos}DsRed^{pos}$ cells (yellow) and the $eGFP^{pos}DsRed^{neg}$ (green) cells in the arterial pole. (**M-R**) Reconstruction of confocal *z*-stacks of *Tg(cmlc2:Kaede)* embryos with the arterial pole of the heart tube to the top. (M-O) *Tg(cmlc2:Kaede)* embryos photoconverted at 19 hpf and imaged at 26 hpf with the green unconverted signal shown in gray in M, the converted red signal in gray in N and a merged image in O. The arrow indicates the location of atrial cells that are green but not red, indicating that they were not expressing the transgene at the time of photoconversion. The dotted line indicates the green signal at 26 hpf. V, ventricle; A, atrium. (P-R) *Tg(cmlc2:Kaede)* embryos photoconverted at 34 hpf and imaged at 48 hpf with the green unconverted signal shown in gray in P, the converted red signal in gray in Q and a merged image in R. Images are of a partial reconstruction of confocal *z*-stacks, allowing a view into the ventricle chamber. The dotted line indicates the green signal at 48 hpf; the arrow in Q indicates the location of distal outflow tract cells that are green but not red, indicating that they were not expressing the transgene at the time of photoconversion.

significant increase in the number of cardiomyocytes was observed (to 311±10, n=5, at 48 hpf; Fig. 1E; see also Table S1 in the supplementary material).

One explanation for the marked increase in cardiomyocyte number could be cell proliferation. To test this hypothesis, serial sections were stained with an antibody recognizing phosphorylated histone (phospho-His). Only a minimal amount of phospho-His staining was present in the myocardium at 30, 36 and 48 hpf, whereas in the surrounding tissues, such as the lateral plate mesoderm, many phospho-His-positive cells were observed (Fig. 1G,H).

To quantify the total number of cardiomyocytes that had undergone at least one round of DNA replication during heart looping, embryos were soaked in a solution containing BrdU from 24 hpf until 48 hpf. When sectioned and stained by an α-BrdU antibody, only 16±2 (n=6) BrdU-positive cardiomyocytes per embryo were observed (Fig. 1I,J; see also Figs S1, S2 in the supplementary material). Surprisingly, 54% of the BrdU-positive cells found in the myocardium were located near the two cardiac poles (within four tiers of cells at the end the myocardial tube), adjacent to the highly proliferating mesenchyme (Fig. 1J). From the BrdU incorporation analysis and the phospho-His staining, we conclude that the low rate of proliferation within the myocardium cannot account for the substantial increase in cardiomyocyte number that we observed in the heart between 24 and 48 hpf.

Distinct phases of cardiomyocyte differentiation at the venous and arterial poles

Our finding that a large fraction of BrdU-positive cells was located near the poles suggested either a local zone of proliferation or the addition and differentiation of cells that originate from the adjacent proliferating mesenchyme to the poles of the heart tube. To investigate cardiomyocyte differentiation, we used a developmental timing assay by examining double transgenic animals expressing both eGFP and DsRed in differentiating cardiomyocytes from the *cardiac myosin light chain 2* (*cmlc2*) promoter

[*Tg(cmlc2:eGFP)/Tg(cmlc2:dsred2-nuc)*]. This approach takes advantage of the observation that the DsRed protein requires more time (approximately 24 hours) to mature and fluoresce than does eGFP, which matures and fluoresces very rapidly (Lepilina et al., 2006; Verkhusha et al., 2001). If cardiomyocyte differentiation occurs at different time points, one would expect to find two populations of cells within the heart myocardium: eGFP^{pos}DsRed^{pos} cells, which have initiated differentiation early, and eGFP^{pos}DsRed^{neg} cells, which have initiated differentiation at a later stage. If cardiomyocyte differentiation occurs at the same time in all cells, one would expect to find a single population of eGFP^{pos}DsRed^{pos} cells.

We could confirm the long maturation time for DsRed protein in the double transgenic embryos [*Tg(cmlc2:eGFP)/Tg(cmlc2:dsred2-nuc)*]. At 24 hpf, the heart tube has formed, and strong eGFP fluorescence was detected in the cardiomyocytes (Fig. 2A). The DsRed fluorescence was still not detectable (Fig. 2B,C), even though antibody staining demonstrated that the DsRed protein was abundantly present at that time (see Fig. S3 in the supplementary material). The DsRed fluorescence was detectable by confocal microscopy only from 36 hpf onwards. Intriguingly, we found two pools of cardiomyocytes, eGFP^{pos}DsRed^{pos} and eGFP^{pos}DsRed^{neg} cells (Fig. 2D-F), suggesting that cardiomyocyte differentiation had indeed occurred in different phases. The eGFP^{pos}DsRed^{pos} cells, which had initiated differentiation early, were located in the ventricle and in a specific region of the atrium (the inner curvature). The eGFP^{pos}DsRed^{neg} cells, which had initiated differentiation at a later time point, were consistently found in the atrium (mainly in the outer curvature) and at the arterial pole (Fig. 2D-F). This is consistent with our observation that the number of *cmlc2*-expressing cells in the lateral plate mesoderm increases gradually over time, with expression in ventricular precursors preceding expression in atrial precursors (see Fig. S4 in the supplementary material). At 48-55 hpf we still observed eGFP^{pos}DsRed^{neg} cells located at both the venous and the arterial poles (Fig. 2G-I). In a single *z*-scan, at the level of the ventricle/outflow region, the different intensities of the eGFP versus the DsRed signal could be appreciated, and is suggestive of the addition of newly differentiating cardiomyocytes at the arterial pole (Fig. 2J-L).

To examine the timing of cardiomyocyte addition in more detail, we employed a transgene [*Tg(cmlc2:kaede)*] in which expression of the red-to-green photoconvertible fluorescent protein Kaede (Ando et al., 2002) is driven by the *cmlc2* promoter. In *Tg(cmlc2:kaede)* embryos, photoconversion of Kaede can mark the differentiated cardiomyocytes present at a specific timepoint: the green form of Kaede in all *cmlc2*-expressing cells converts into the red form, labeling these cells with red fluorescence even as they continue to produce additional green Kaede (see Fig. S5 in the supplementary material). By contrast, newly differentiating cells that begin expressing *cmlc2* after the time of photoconversion will fluoresce green, but not red (Fig. S5 in the supplementary material).

Photoconversion at 34 hpf, followed by examination of fluorescence at 48 hpf, revealed a population of green, but not red, cardiomyocytes at the distal portion of the arterial pole, indicating the addition of these cells between 34 and 48 hpf (*n*=8/8; Fig. 2P-R; see also Fig. S5 in the supplementary material). However, we did not observe the addition of cardiomyocytes to the venous pole during the same timeframe (*n*=8/8; see Fig. S5 in the supplementary material). Instead, the addition of atrial cells seems to occur at earlier stages. Photoconversion at 19 hpf, followed by examination at 26 hpf, demonstrated that cardiomyocytes are added to a portion of the atrium (its future outer curvature) following the initial differentiation of the ventricle and the future atrial inner curvature (*n*=4/4; Fig. 2M-O). In these embryos, we did not observe any cells being added to the arterial pole. Synchronizing these data with the results of our developmental timing assays, we find a defined sequence for cardiomyocyte differentiation in zebrafish. An initial wave of differentiation begins with the formation of the ventricle and continues to gradually create the atrium; subsequently, additional cardiomyocytes are appended to the arterial pole.

Islet1 mutants have reduced cardiomyocyte differentiation at the venous pole

Next we wanted to identify the signals that regulate these two waves of cardiomyocyte differentiation. Islet 1 (*Isl1*) deficient mouse embryos lack part of the atria and most of the outflow tract and right ventricle, suggesting that *Isl1*-expressing cells contribute to both the venous and the arterial poles of the mouse heart (Cai et al., 2003). More recent studies demonstrated that *Isl1* is expressed throughout the heart (Prall et al., 2007), and is also required for heart morphogenesis and early cardiomyocyte specification in *Drosophila* and *Xenopus*, respectively (Brade et al., 2007; Tao et al., 2007). To identify a possible *isl1*-positive cardiac progenitor cell population in the zebrafish, we analyzed expression at various stages. Using an antibody recognizing both Isl1 and Isl2 proteins (Hutchinson and Eisen, 2006; Wan et al., 2006), we observed a strong nuclear signal in the trigeminal sensory ganglia, the vascular endothelium, and the endoderm, which lays dorsal to the cardiac field (Trinh Le and Stainier, 2004) (Fig. 3B,C). We also observed a nuclear signal in cells located at the periphery of the cardiac field where future atrial cells are located (Fig. 3A-F; see Fig. S6 in the supplementary material). Frequently the Isl-positive cells also expressed *Tg(cmlc2:eGFP)*, indicating that cardiomyocyte differentiation had been initiated in the Isl-positive cells.

To address whether zebrafish Isl1 is required for normal heart development, we screened for mutant alleles in an ENU-mutagenized library (Wienholds et al., 2002). We identified one allele that results in a premature stop codon in the third exon, removing part of the LIM-domain and the entire homeobox (Fig. 4A,B). At 24 hpf, the *isl1* mutant embryos look morphologically normal but are immotile, which can be explained by the function of

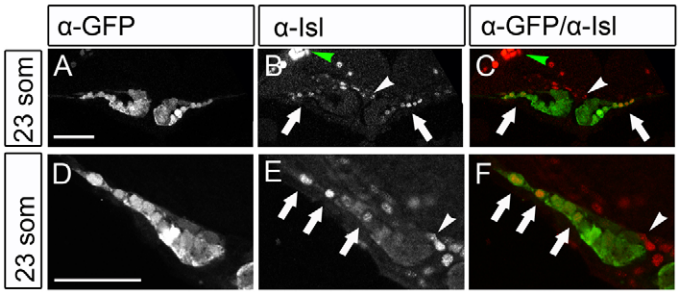

Fig. 3. Isl localization in cardiomyocytes of the future atrium. (**A-F**) Isl is expressed in cardiac cells located at lateral positions in the cardiac disk. Single *z*-scans of confocal images of *Tg(cmlc2:eGFP)* embryos at 23 somites immunofluorescently stained with α-eGFP and α-Isl antibodies. C and F show an overlay with eGFP in green and Isl in red. Images in D-F are magnified views of one side of the cardiac disk. Arrows indicate the eGFP^{pos}Isl^{pos} cells located at lateral positions (future atrium) of the cardiac disk. The white arrowhead indicates Isl-positive cells in the endocardium and the green arrowhead indicates the Isl signal in the trigeminal sensory ganglion. Scale bars: 50 μm.

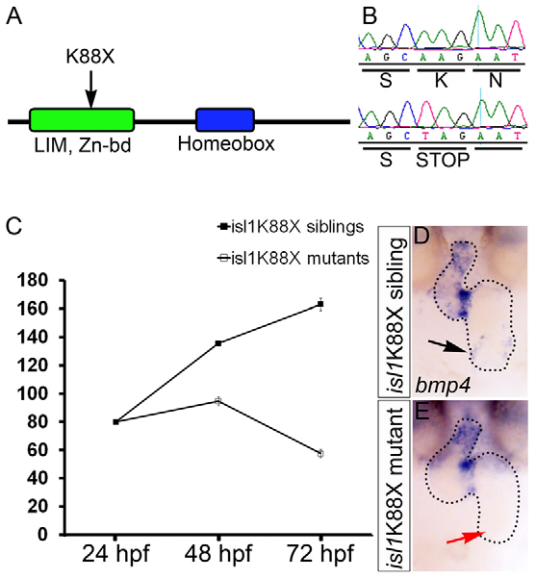

Fig. 4. Cardiac defects of *isl1*^{K88X} mutant embryos. (**A**) Cartoon of the Isl1 protein with the location of the premature stop codon (K88X) identified in the *isl1* mutant. (**B**) DNA sequence of a homozygous wild-type sibling (top) and a homozygous *isl1*^{K88X} mutant (bottom) at the site of the mutation (AAG>TAG) that results in a premature stop codon. (**C**) The number of heart beats per minute measured at 24, 48 and 72 hpf of wild-type sibling (black squares) and *isl1* mutant (white squares) embryos. (**D**,**E**) In situ hybridization for *bmp4* on 48 hpf wild-type sibling (D) and *isl1* mutant (E) embryos. Black arrow (D) indicates *bmp4* expression in the sinus venosus of a wild-type embryo; red arrow (E) indicates the inflow area of a representative *isl1* mutant embryo lacking *bmp4* expression. Embryos are shown as frontal-ventral views (OFT to the top).

Isl1 described in primary motoneurons (Hutchinson and Eisen, 2006) (see Fig. S7A-D in the supplementary material; data not shown). In addition to the motility defect, the heart of *isl1* mutant embryos contracts irregularly and with a reduced frequency (bradycardia; Fig. 4C). Whereas the heart frequency in wild-type siblings will rise from 80±1 beats/minute at 24 hpf to 163±4 beats/minute at 48 hpf, the heart frequency of *isl1* mutants remains low (95±3 beats/minute at 48 hpf, 58±3 beats/minute at 72 hpf; see Table S2 in the supplementary material). In addition, *isl1* mutant hearts showed frequent pauses in the cardiac contraction, resulting in reduced blood circulation in the trunk and tail (see Movie 1 in the supplementary material). Subsequently, *isl1* mutant larvae die between 5 and 7 dpf.

To identify a possible cause for the cardiac defects observed in *isl1* mutant embryos, we performed in situ hybridizations with several cardiac marker genes. Although *nkx2.5* and *cmlc2* were normally expressed, *bmp4* expression was clearly affected in *isl1* mutants (Fig. 4D,E; data not shown). In wild-type siblings, *bmp4* was expressed in the OFT, the atrioventricular canal (AVC) and the sinus venosus (SV). Surprisingly, although *bmp4* expression in the OFT and the AVC was unaffected in *isl1* mutants, *bmp4* expression in the SV was completely abolished.

To address whether the observed cardiovascular defects in *isl1* mutant embryos could result from a defect in cardiomyocyte differentiation, we used the above-described developmental timing assay. To do so, we crossed the *isl1* mutation into *Tg(cmlc2:eGFP)/Tg(cmlc2:dsred2-nuc)* double transgenic embryos and quantified the number of eGFP^{pos}DsRed^{pos} cardiomyocytes and eGFP^{pos}DsRed^{neg} cardiomyocytes in confocal images after 3D reconstruction (Fig. 5A-F). We observed no significant difference in the number of eGFP^{pos}DsRed^{pos} cells (siblings, 200±6; mutants, 203±7) nor in the number of eGFP^{pos}DsRed^{neg} cells at the arterial pole (sibs, 28±1; mutants, 32±2; Fig. 5G-K; see also Table S3 in the supplementary material), demonstrating that cardiomyocyte differentiation still occurs. We did, however, observe a significant reduction in the number of eGFP^{pos}DsRed^{neg} cells at the venous pole of *isl1* mutants (25±3 in sibling hearts and 10±3 in mutant hearts, $P<0.01$; Fig. 5D-F,K). To confirm that the observed defects in cardiomyocyte differentiation resulted from the loss of Isl1 function, we used antisense morpholinos (MO) against *isl1*, which affect splicing of the *isl1* mRNA and thereby prevent Isl1 protein production (Hutchinson and Eisen, 2006) (see Fig. S8 in the supplementary material). Using the developmental timing assay, we again observed a significant reduction in the number of eGFP^{pos}DsRed^{neg} cells at the venous pole, while the number of eGFP^{pos}DsRed^{neg} cells at the arterial pole remained unaffected. The stronger effects on cardiac morphology and the number of eGFP^{pos}DsRed^{pos} cells observed after *isl1* MO injection were probably due to an additional toxic effect of the MO injection.

Because *isl1* mutant embryos display cardiac dysfunction, we addressed whether cardiac dysfunction by itself can affect cardiomyocyte addition. To interfere with cardiac function, we injected *tnnt2* MOs (Sehnert et al., 2002). Although cardiac contraction was abolished in *tnnt2* Mo-injected embryos, the addition of new cardiomyocytes to both poles of the heart tube was not significantly altered (see Fig. S9 in the supplementary material).

In conclusion, the loss of *bmp4* expression in the SV combined with the reduced number of eGFP^{pos}DsRed^{neg} cardiomyocytes at the venous pole demonstrate that, in zebrafish, Isl1 is specifically required to complete cardiomyocyte differentiation at the venous pole and not at the arterial pole. This suggests that other, Isl1-independent pathways regulate the addition of cardiomyocytes to the arterial pole (see Discussion).

Fgf signaling is required for cardiomyocyte addition at the arterial pole

Two previous studies using conditional and hypomophic *Fgf8* alleles in mouse have demonstrated that Fgf signaling is crucial for the recruitment of SHF cells to the arterial pole of the heart (Ilagan et al., 2006; Park et al., 2006). Consistent with the suggested role for *fgf8* in arterial pole formation, the zebrafish *fgf8* mutation *acerebellar* (*ace*) is known to diminish the size of the ventricle (Reifers et al., 2000). Furthermore, inhibition of Fgf signaling between 24 and 48 hpf reduces the number of ventricular cardiomyocytes in the zebrafish heart, but the cellular mechanism responsible for this deficiency has not yet been elucidated (Marques et al., 2008). To address whether Fgf signaling is activated at the arterial pole, we analyzed *sprouty4* (*spry4*) expression at stages between 24 and 48 hpf, because Sprouty proteins are Fgf antagonists that are induced by Fgf signaling (Furthauer et al., 2001; Hacohen et al., 1998). At 24 hpf, we observed very strong *spry4* expression at the midbrain-hindbrain boundary and much weaker expression near the arterial pole of the linear heart tube (Fig. 6A,B). At 36 hpf, *spry4* expression was observed in the heart tube and at the position where the arterial pole connects to the head mesoderm (Fig. 6C). Speculating that Fgf8 might regulate the addition of cells to the arterial pole of the zebrafish heart tube, we injected the eGFP/DsRed double transgenic embryos with an antisense MO targeting *fgf8* and

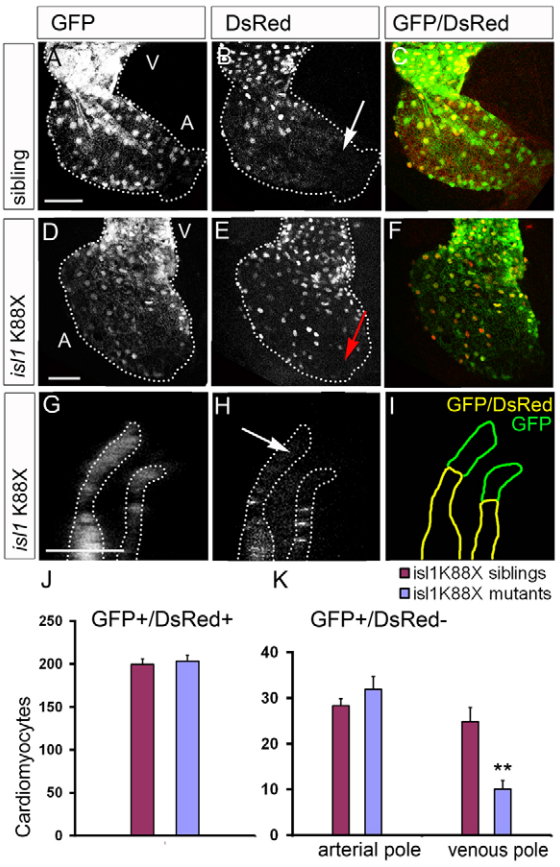

Fig. 5. Reduced cardiomyocyte differentiation at the venous pole in *isl1* mutant embryos. (**A-F**) Single *z*-scan of the atrium of a representative *isl1*^{K88X} sibling (A-C) and mutant (D-F) embryo. White arrow (B) indicates eGFP^{pos}DsRed^{neg} cardiomyocytes at the venous pole of the wild-type sibling heart; red arrow (E) indicates the venous pole of the *isl1* mutant where only very few eGFP^{pos}DsRed^{neg} cells are present. (**G**,**H**) Single *z*-scan of a confocal image at the level of the arterial pole showing the eGFP^{pos}DsRed^{neg} cardiomyocytes in the *isl1* mutant (white arrow). The region shown is similar to that of the control embryo shown in Fig. 2G-I. V, ventricle: A, atrium. Scale bar: 50 μm. (**I**) Schematic of the location of the eGFP^{pos}DsRed^{pos} cells (yellow) and the eGFP^{pos}DsRed^{neg} (green) cells in the arterial pole of the *isl1* mutant. (**J**,**K**) The number of eGFP^{pos}DsRed^{pos} (J) and eGFP^{pos}DsRed^{neg} (K) cardiomyocytes per embryo. (K) The eGFP^{pos}DsRed^{neg} cardiomyocytes are subdivided into eGFP^{pos}DsRed^{neg} cells being present at either the arterial or the venous pole. Note the significant reduction of eGFP^{pos}DsRed^{neg} cells at the venous pole in the *isl1* mutants. Bars represent mean±s.e.m. $^{**}P<0.01$.

reproducing the *ace/fgf8* mutant phenotypes (see Fig. S10 in the supplementary material) (Draper et al., 2001). In agreement with the reported role of Fgf signaling in cardiomyocyte specification, the hearts of *fgf8* MO-injected embryos were much smaller than those of wild type, and we found that the total number of myocardial cells was significantly decreased (control, 305±23, *n*=3; *fgf8* MO, 196±6, *n*=4; $P<0.05$; Fig. 6E-G,N). In addition, a significant reduction in the number of eGFP^{pos}DsRed^{neg} cells at the arterial pole was observed (control, 29±1, *n*=3; *fgf8* MO, 17±4, *n*=4; $P<0.05$), while the number of eGFP^{pos}DsRed^{neg} cells at the venous pole did not change significantly (control, 32±4, *n*=3; *fgf8* MO, 26±2, *n*=4; Fig. 6N,O; see also Table S3 in the supplementary material).

Next, we used the Fgfr inhibitor SU5402 to address the temporal requirement for Fgf signaling during the addition of cells to the arterial pole. SU5402 efficiently blocked Fgf signaling (Fig. 6C,D). Double eGFP/DsRed transgenic embryos were treated from 24 hpf until 48 hpf with SU5402, and eGFP^{pos}DsRed^{pos} and eGFP^{pos}DsRed^{neg} cells were quantified. In SU5402-treated embryos, the number of eGFP^{pos}DsRed^{pos} cells was unchanged, indicating normal cardiomyocyte specification (Fig. 6H-J,N; see also Table S3 in the supplementary material). Furthermore, the number of eGFP^{pos}DsRed^{neg} cells at the venous pole of the SU5402-treated embryos was equal to the number of eGFP^{pos}DsRed^{neg} cells in DMSO-treated embryos (DMSO, 30±1, *n*=3; SU5402, 31±3, *n*=5; Fig. 6O). By contrast, the number of eGFP^{pos}DsRed^{neg} cells at the arterial pole of SU5402-treated embryos was significantly reduced (DMSO, 30±4, *n*=3; SU5402, 6±2, *n*=5; $P<0.01$; Fig. 6K-M,O). Together, these results demonstrate that Fgf signaling between 24 and 48 hpf is required for the addition of new cardiomyocytes to the arterial pole of the zebrafish heart.

DISCUSSION

By using live imaging in the zebrafish model, we have been able to visualize the dynamics of cardiomyocyte differentiation in a vertebrate embryo, revealing distinct phases of cardiomyocyte differentiation. Both the GFP/DsRed developmental timing assay and the Kaede photoconversion experiments demonstrated that the cardiomyocytes of the future ventricle are the first to differentiate. New cardiomyocytes are added to the heart by two distinct phases of cardiomyocyte differentiation. First, a cardiomyocyte differentiation program starting in the ventricle and progressing along the atrium allows the continuous addition of new cardiomyocytes to the venous pole of the heart tube. At the arterial pole, a second phase of cardiomyocyte differentiation that is temporally distinct from the initial phase of cardiomyocyte differentiation was observed. This population of cells forming from the second phase of differentiation will contribute to the outflow tract. In addition to this separation in time and space (venous versus arterial pole, respectively), we also demonstrated differences in the regulation of the two phases of cardiomyocyte differentiation.

Cardiomyocyte differentiation at the venous pole

By using two different assays, developmental timing and Kaede photoconversion, we demonstrated that cardiomyocyte differentiation is initiated in the ventricle. Subsequently, atrial cells are added at the venous pole by a continuation of cardiomyocyte differentiation. These results are in agreement with the previous findings in both chick and zebrafish that the induction of atrium-specific myosin gene expression occurs after the induction of ventricle-specific myosin expression (Berdougo et al., 2003; Yutzey et al., 1994). Our Kaede photoconversion experiments demonstrate that the differentiation at the venous pole is completed by 34 hpf at the latest. Finally, our results demonstrate that Isl1 is required to complete the cardiomyocyte differentiation process at the venous pole. Interestingly, we observed bradycardia and frequent pauses in cardiac contraction in the zebrafish *isl1* mutant embryos. This was not reported for the mouse *Isl1* mutants, which could have been because of the severe heart failure observed in these embryos (Cai et al., 2003). Earlier experiments in chick demonstrated that intrinsic heart beat frequency increases over the anteroposterior axis and that a single pacemaker area becomes established at the venous pole (Moorman et al., 1998). Problems in pacemaker activity result in a so-called sick sinus syndrome, which is characterized by arrhythmias, such as sinus bradycardia and sinus pauses, or arrests

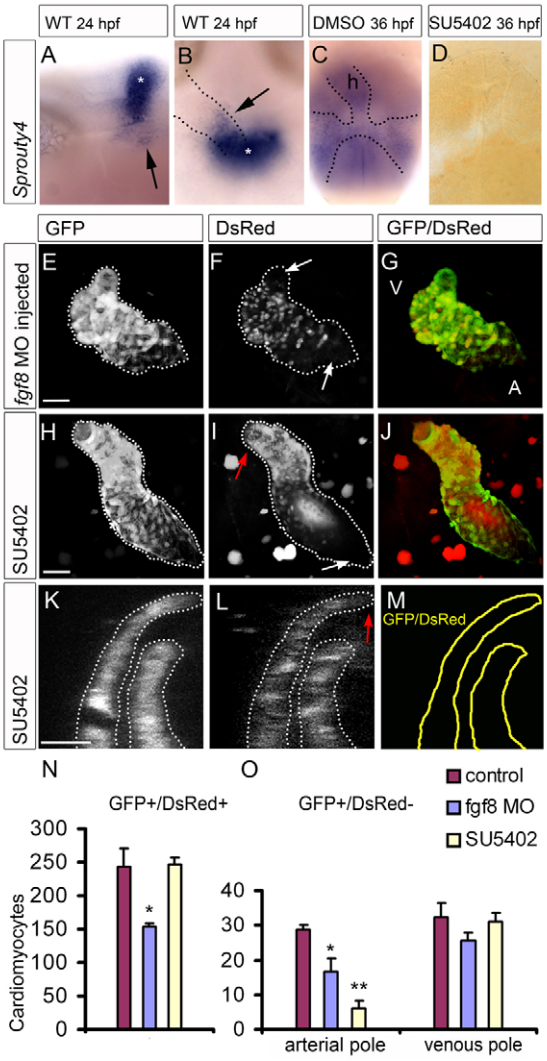

Fig. 6. Fgf signaling is required for the addition of cardiomyocytes to the arterial pole. (**A-D**) In situ hybridization for *sprouty4* (*spry4*). (A,B) Lateral (A) and dorsal (B) view of a 24 hpf embryo. The arrows indicate the region of *spry4* expression near the arterial pole of the heart tube, which could contribute cells to the heart tube. The asterisk indicates the midbrain-hindbrain boundary. In B the heart tube is indicated by the dotted line. (C,D) Dorsal views of 36 hpf embryos that had been treated from 24 hpf until 36 hpf with DMSO (C) or SU5402 (D); *spry4* expression in the DMSO-treated embryo is outlined by the dotted line. (**E-J**) Images of the developmental timing assay (similar to Fig. 2A-I). The arterial pole is at the top left. V, ventricle; A, atrium. The dotted line outlines the eGFP-positive heart tubes. Scale bars: 50 μm. (E-G) A representative *fgf8* MO-injected embryo showing reduced heart size. The white arrows indicate the $eGFP^{pos}DsRed^{neg}$ cells at the poles of the heart. (H-J) A representative embryo treated with SU5402 from 24-48 hpf. The red arrow indicates the arterial pole, in which $eGFP^{pos}DsRed^{neg}$ are absent; the white arrow indicates the $eGFP^{pos}DsRed^{neg}$ cells at the venous pole. The peripheral red dots are background signal from yolk granules; the diffuse red signal within the heart tube is due to background fluorescence of red blood cells accumulated within the heart lumen. (**K**,**L**) Single *z*-scan of a confocal image taken from a *Tg(cmlc2:eGFP)/Tg(cmlc2:dsred2-nuc)* embryo treated with SU5402 from 24-48 hpf. A complete overlap of the eGFP (K) and DsRed (L) signals at the distal tip of the outflow (red arrow) was observed, in contrast to the control embryos represented in Fig. 2J,K. Scale bar: 25 μm. (**M**) Schematic of the location of the $eGFP^{pos}DsRed^{pos}$ cells after SU5402 treatment. (**N**,**O**) The number of $eGFP^{pos}DsRed^{pos}$ (N) and $eGFP^{pos}DsRed^{neg}$ (O) cardiomyocytes/embryo. (O) The $eGFP^{pos}DsRed^{neg}$ cardiomyocytes are subdivided into those present at the arterial pole and those present at the venous pole. Bars represent mean±s.e.m. Note the reduction in the number of $eGFP^{pos}DsRed^{neg}$ cells located at the arterial pole after *fgf8* MO-injection or SU5402 treatment. $*P<0.05$; $**P<0.01$.

(Dobrzynski et al., 2007). Therefore, the reduced heart frequency and the pauses in contraction that we observed in *isl1* mutant embryos could be explained by a failure of cardiomyocyte differentiation at the venous pole. Indeed, we observed a specific loss of *bmp4* expression and a significant reduction in the number of $eGFP^{pos}DsRed^{neg}$ cells at the venous pole, which demonstrated reduced cardiomyocyte differentiation at the venous pole. One explanation for the residual cardiomyocyte differentiation observed in *isl1* mutant embryos could be that Isl1 is redundant with other Islet factors during cardiomyocyte differentiation. Because the α-Isl antibody we used can recognize both Isl1 and Isl2 proteins, and because almost all signal is lost in the *isl1* mutant (see Fig. S7 in the supplementary material), we do not believe this to be a likely explanation. An alternative explanation would be that Isl1 is required for the differentiation of a specific subset of cardiomyocytes located at the venous pole. As Isl1 is expressed in various cell types near and in the differentiating cardiomyocytes (Fig. 3), the autonomy of Isl1 during cardiomyocyte addition at the venous pole remains an open and interesting question.

Contrary to an earlier study in *Xenopus* in which it was demonstrated that Isl1 knockdown affects differentiation of all cardiomyocytes (Brade et al., 2007), we did not observe any effect on the expression of early cardiac markers (e.g. *nkx2.5*) in *isl1* mutant or *isl1* MO-injected embryos (E.d.P. and J.B., unpublished observations).

From our observations in zebrafish, Mouse Isl1 seems to have a much broader function than does zebrafish Isl1. Mouse Isl1 is required for the recruitment of cells to both the venous pole (both atria) and the arterial pole (right ventricle and OFT) (Cai et al., 2003). Possible explanations for these differences could be that at the arterial pole zebrafish Isl1 is redundant with other Islet factors, which, from the arguments described above, we do not believe to be likely. An alternative and more likely explanation would be that these differences reflect evolutionary differences between teleosts and amniotes, differences that are responsible for the recruitment of the extra cardiomyocytes required to form additional chambers (see also below).

Cardiomyocyte differentiation at the arterial pole

The Kaede photoconversion experiments demonstrate that there is discontinuity between the initial phase of differentiation, which gives rise to cardiomyocytes that form the ventricle and atrium, and the later addition of cells to the arterial pole. At 19-26 hpf, when cardiomyocytes are still added to the venous pole, addition of new cardiomyocytes to the arterial pole was hardly observed. Addition of new cardiomyocytes at the arterial pole was apparent only at later stages of cardiac development (34-48 hpf). Interestingly, BrdU labeling in chick has revealed a population of labeled cardiomyocytes at the venous pole at stage 10, when no such cells

were evident at the arterial pole (Soufan et al., 2006). It was suggested that these venous pole cells had incorporated BrdU in the splanchnic mesoderm before being added to the venous pole. Together with the observation that cells are not added to the arterial pole until after stage 12 (de la Cruz et al., 1977; Mjaatvedt et al., 2001), this would suggest that cardiomyocyte differentiation at the venous pole is occurring much earlier than differentiation at the arterial pole in chick embryos. However, the visualization of cardiomyocyte differentiation in mouse or chick embryos would be required to allow a direct comparison of the dynamics.

Our data demonstrate that cardiomyocyte differentiation at the arterial pole is independent of Isl1 but requires Fgf8 signaling. The small ventricle previously observed in *ace/fgf8* mutant fish and the small ventricle generated by blocking Fgf signaling at the linear heart tube stage (Marques et al., 2008; Reifers et al., 2000) can now be explained by diminished cardiomyocyte differentiation at the arterial pole. The differences that we observe after *fgf8*-MO injection or SU5402 treatment can be explained by a difference in timing when Fgf signaling is blocked by these different treatments (Marques et al., 2008). In the case in which Fgf8 signaling is inhibited by the MO injection, Fgf8 signaling is inhibited already at very early stages during cardiomyocyte specification, which provides an explanation for the reduction in the number of $eGFP^{pos}DsRed^{pos}$ cells we observed. In the case of SU5402 treatment, we added the inhibitor only at the tube stage (24 hpf), and therefore this treatment affects only later cardiomyocyte addition. Whether these two phases of Fgf requirement during cardiomyocyte differentiation also exist in other vertebrates has been difficult to address owing to the early lethality of mouse mutants with reduced Fgf signaling during gastrulation (Dono et al., 1998; Feldman et al., 1995; Meyers et al., 1998). However, by using different conditional *Fgf8* mutant alleles, Park et al. showed that the early loss of Fgf8 affects both ventricle and atrium formation, whereas the late and specific deletion of *Fgf8* in the anterior heart field specifically affects the OFT (Park et al., 2006).

Surprisingly, cardiomyocyte differentiation in zebrafish at the arterial pole does not require Isl1 (also discussed above). This demonstrates that not only is the temporal regulation of cardiomyocyte differentiation at both poles different, but also the mechanism and signals involved in regulating cardiomyocyte differentiation are different at each pole of the zebrafish heart.

Evolutionary adaptation

Our observation that cardiomyocyte differentiation at the arterial pole is temporally separated from and regulated differently to the continuous wave of differentiation in the rest of the heart tube may also help to explain the different phenotypes (broad heart defects versus OFT defects) observed in several mouse mutants. Mice deficient for *Isl1* display broad cardiac defects that affect the formation of ventricles as well as atria (Cai et al., 2003). We now suggest that the role for Isl1, which is required to complete the continuous differentiation process in zebrafish, has been expanded in amniotes to increase the relative size of the heart. Interestingly, during growth of the heart tube in amniotes, both the venous and the arterial pole remain connected to the dorsal mesocardium, where Isl1 is expressed. In zebrafish, however, the Isl1-positive cells located laterally in the cardiac field are physically separated from the future ventricle cells that are located medially in the cardiac field.

Taken together, our results demonstrate that two distinct phases of cardiomyocyte differentiation contribute to the observed growth of the embryonic heart. This is the first time that the temporal regulation of cardiomyocyte differentiation has been visualized in any vertebrate organism. We believe that this new concept of two separate phases of cardiomyocyte differentiation that require different molecular mechanisms for their completion provides new insight into how the vertebrate heart grows and could have expanded during vertebrate evolution.

We thank Dr Cuppen (Hubrecht Laboratory) and Dr Stemple (Welcome Trust Sanger Institute) for providing the *isl1*^{k88x} zebrafish mutant, which was generated as part of the ZF-MODELS Integrated Project in the 6th Framework Programme (Contract No. LSHG-CT-2003-503496) funded by the European Commission. We also thank R. Kelly for discussions and suggestions when this work was in progress, K. Poss for providing the *Tg(cmlc2:dsred2-nuc)* fish, A. Moorman and K. Smith for critical reading of the manuscript and members of the Bakkers laboratory for stimulating discussions. Work in J.B.'s laboratory was supported by the Royal Dutch Academy of Arts and Sciences. Work in D.Y.'s laboratory was supported by the National Institutes of Health. E.d.P. was supported by EU FP6 grant LSHM-CT-2005-018833, EUGeneHeart. S.M. was supported by the GABBA program and the Portuguese Foundation for Science and Technology (POCI 2010-FSE). Deposited in PMC for release after 12 months.

Supplementary material

Supplementary material for this article is available at http://dev.biologists.org/cgi/content/full/136/10/1633/DC1

References

Ando, R., Hama, H., Yamamoto-Hino, M., Mizuno, H. and Miyawaki, A. (2002). An optical marker based on the UV-induced green-to-red photoconversion of a fluorescent protein. *Proc. Natl. Acad. Sci. USA* **99**, 12651-12656.

Berdougo, E., Coleman, H., Lee, D. H., Stainier, D. Y. and Yelon, D. (2003). Mutation of weak atrium/atrial myosin heavy chain disrupts atrial function and influences ventricular morphogenesis in zebrafish. *Development* **130**, 6121-6129.

Brade, T., Gessert, S., Kuhl, M. and Pandur, P. (2007). The amphibian second heart field: Xenopus islet-1 is required for cardiovascular development. *Dev. Biol.* **311**, 297-310.

Buckingham, M. E., Meilhac, S. and Zaffran, S. (2005). Building the mammalian heart from two sources of myocardial cells. *Nat. Rev. Genet.* **6**, 826-835.

Cai, C. L., Liang, X., Shi, Y., Chu, P. H., Pfaff, S. L., Chen, J. and Evans, S. (2003). Isl1 identifies a cardiac progenitor population that proliferates prior to differentiation and contributes a majority of cells to the heart. *Dev. Cell* **5**, 877-889.

de la Cruz, M. V., Sanchez, G. C., Arteaga, M. M. and Arguello, C. (1977). Experimental study of the development of the truncus and the conus in the chick embryo. *J. Anat.* **123**, 661-686.

Dobrzynski, H., Boyett, M. R. and Anderson, R. H. (2007). New insights into pacemaker activity: promoting understanding of sick sinus syndrome. *Circulation* **115**, 1921-1932.

Dono, R., Texido, G., Dussel, R., Ehmke, H. and Zeller, R. (1998). Impaired cerebral cortex development and blood pressure regulation in Fgf2 deficient mice. *EMBO J.* **17**, 4213-4225.

Draper, B. W., Morcos, P. A. and Kimmel, C. B. (2001). Inhibition of zebrafish fgf8 pre-mRNA splicing with morpholino oligos: a quantifiable method for gene knockdown. *Genesis* **30**, 154-156.

Feldman, B., Poueymirou, W., Papaioannou, V. E., DeChiara, T. M. and Goldfarb, M. (1995). Requirement for Fgf-4 for postimplantation mouse development. *Science* **267**, 246-249.

Fisher, S., Grice, E. A., Vinton, R. M., Bessling, S. L., Urasaki, A., Kawakami, K. and McCalion, A. S. (2006). Evaluating the biological relevance of putative enhancers using Tol2 transposon-mediated transgenesis in zebrafish. *Nat. Protoc.* **1**, 1297-1305.

Furthauer, M., Reifers, F., Brand, M., Thisse, B. and Thisse, C. (2001). sprouty4 acts in vivo as a feedback-induced antagonist of FGF signaling in zebrafish. *Development* **128**, 2175-2186.

Hacohen, N., Kramer, S., Sutherland, D., Hiromi, Y. and Krasnow, M. A. (1998). sprouty encodes a novel antagonist of FGF signaling that patterns apical branching of the Drosophila airways. *Cell* **92**, 253-263.

Hatta, K., Tsujii, H. and Omura, T. (2006). Cell tracking using a photoconvertible fluorescent protein. *Nat. Protoc.* **1**, 960-967.

Huang, C. J., Tu, C. T., Hsiao, C. D., Hsieh, F. J. and Tsai, H. J. (2003). Germ-line transmission of a myocardium-specific GFP transgene reveals critical regulatory elements in the cardiac myosin light chain 2 promoter of zebrafish. *Dev. Dyn.* **228**, 30-40.

Hutchinson, S. A. and Eisen, J. S. (2006). Islet1 and Islet2 have equivalent abilities to promote motoneuron formation and to specify motoneuron subtype identity. *Development* **133**, 2137-2147.

Ilagan, R., Abu-Issa, R., Brown, D., Yang, Y. P., Jiao, K., Schwartz, R. J., Klingensmith, J. and Meyers, E. N. (2006). Fgf8 is required for anterior heart field development. *Development* **133**, 2435-2445.
Kelly, R. G., Brown, N. A. and Buckingham, M. E. (2001). The arterial pole of the mouse heart forms from Fgf10-expressing cells in pharyngeal mesoderm. *Dev. Cell* **1**, 435-440.
Lepilina, A., Coon, A. N., Kikuchi, K., Holdway, J. E., Roberts, R. W., Burns, C. G. and Poss, K. D. (2006). A dynamic epicardial injury response supports progenitor cell activity during zebrafish heart regeneration. *Cell* **127**, 607-619.
Mably, J. D., Mohideen, M. A., Burns, C. G., Chen, J. N. and Fishman, M. C. (2003). heart of glass regulates the concentric growth of the heart in zebrafish. *Curr. Biol.* **13**, 2138-2147.
Marques, S. R., Lee, Y., Poss, K. D. and Yelon, D. (2008). Reiterative roles for FGF signaling in the establishment of size and proportion of the zebrafish heart. *Dev. Biol.* **321**, 397-406.
Meyers, E. N., Lewandorski, M. and Martin, G. R. (1998). An Fgf8 mutant allelic series generated by Cre- and Flp-mediated recombination. *Nat. Genet.* **18**, 136-142.
Mjaatvedt, C. H., Nakaoka, T., Moreno-Rodriguez, R., Norris, R. A., Kern, M. J., Eisenberg, C. A., Turner, D. and Markwald, R. R. (2001). The outflow tract of the heart is recruited from a novel heart-forming field. *Dev. Biol.* **238**, 97-109.
Moorman, A. F., Christoffels, V. M., Anderson, R. H. and van den Hoff, M. J. (2007). The heart-forming fields: one or multiple? *Philos. Trans. R. Soc. Lond. B Biol. Sci.* **362**, 1257-1265.
Moorman, A. F., de Jong, F., Denyn, M. M. and Lamers, W. H. (1998). Development of the cardiac conduction system. *Circ. Res.* **82**, 629-644.
Park, E. J., Ogden, L. A., Talbot, A., Evans, S., Cai, C. L., Black, B. L., Frank, D. U. and Moon, A. M. (2006). Required, tissue-specific roles for Fgf8 in outflow tract formation and remodeling. *Development* **133**, 2419-2433.
Prall, O. W., Menon, M. K., Solloway, M. J., Watanabe, Y., Zaffran, S., Bajolle, F., Biben, C., McBride, J. J., Robertson, B. R., Chaulet, H. et al. (2007). An Nkx2-5/Bmp2/Smad1 negative feedback loop controls heart progenitor specification and proliferation. *Cell* **128**, 947-959.
Reifers, F., Walsh, E. C., Leger, S., Stainier, D. Y. and Brand, M. (2000). Induction and differentiation of the zebrafish heart requires fibroblast growth factor 8 (fgf8/acerebellar). *Development* **127**, 225-235.
Sehnert, A. J., Huq, A., Weinstein, B. M., Walker, C., Fishman, M. and Stainier, D. Y. (2002). Cardiac troponin T is essential in sarcomere assembly and cardiac contractility. *Nat. Genet.* **31**, 106-110.
Smith, K. A., Chocron, S., von der Hardt, S., de Pater, E., Soufan, A., Bussmann, J., Schulte-Merker, S., Hammerschmidt, M. and Bakkers, J. (2008). Rotation and asymmetric development of the zebrafish heart requires directed migration of cardiac progenitor cells. *Dev. Cell* **14**, 287-297.
Soufan, A., van den Berg, G., Ruijter, J. M., de Boer, P. A. J., van den Hoff, M. J. and Moorman, A. F. (2006). Regionalized sequence of myocardial cell growth and proliferation characterizes early chamber formation. *Circ. Res.* **99**, 545-552.
Tao, Y., Wang, J., Tokusumi, T., Gajewski, K. and Schulz, R. A. (2007). Requirement of the LIM homeodomain transcription factor tailup for normal heart and hematopoietic organ formation in Drosophila melanogaster. *Mol. Cell. Biol.* **27**, 3962-3969.
Trinh Le, A. and Stainier, D. Y. (2004). Fibronectin regulates epithelial organization during myocardial migration in zebrafish. *Dev. Cell* **6**, 371-382.
Verkhusha, V. V., Otsuna, H., Awasaki, T., Oda, H., Tsukita, S. and Ito, K. (2001). An enhanced mutant of red fluorescent protein DsRed for double labeling and developmental timer of neural fiber bundle formation. *J. Biol. Chem.* **276**, 29621-29624.
Waldo, K. L., Kumiski, D. H., Wallis, K. T., Stadt, H. A., Hutson, M. R., Platt, D. H. and Kirby, M. L. (2001). Conotruncal myocardium arises from a secondary heart field. *Development* **128**, 3179-3188.
Wan, H., Korzh, S., Li, Z., Mudumana, S. P., Korzh, V., Jiang, Y. J., Lin, S. and Gong, Z. (2006). Analyses of pancreas development by generation of gfp transgenic zebrafish using an exocrine pancreas-specific elastaseA gene promoter. *Exp. Cell Res.* **312**, 1526-1539.
Westerfield, M. (1995). *The Zebrafish Book*. Oregon: University of Oregon Press.
Wienholds, E., Schulte-Merker, S., Walderich, B. and Plasterk, R. H. A. (2002). Target-selected inactivation of the zebrafish *rag1* gene. *Science* **297**, 99-102.
Yutzey, K. E., Rhee, J. T. and Brader, D. (1994). Expression of the atrial-specific myosin heavy chain AMHC1 and the establishment of anteroposterior polarity in the developing chicken heart. *Development* **120**, 871-883.

Table S1. Cardiomyocyte number at various stages

Stage	Cardiomyocytes*	*n*
24 hpf	150.6±11.5	5
36 hpf	213.2±11.7	5
48 hpf	310.6±9.7	5

*As determined by α-DsRed antibody staining in *Tg(cmlc2:DsRed)* embryos. Values are mean±s.e.m.

Table S2. Heartbeats per minute

Stage	24 hpf	48 hpf	72 hpf	*n*
isl1^{K88X} siblings	80±1.3	135.5±1.8	163±4.4	5
isl1^{K88X} mutants	80±1.3	94.6±3.2*	57.5±2.9*	10

**P*<0.01.
Values are mean±s.e.m.

Table S3. Cell count of GFP^{pos}/DsRed^{pos} and GFP^{pos}/DsRed^{neg} myocardial cells

		GFP^{pos}/DsRed^{neg}			
Treatment	GFP^{pos}/DsRed^{pos}	Arterial pole	Venous pole	Total	*n*
isl1^{K88X} siblings	199.7±6.2	28.4±1.5	24.9±3.1	253±9.2	7
isl1^{K88X} mutants	203.3±7.1	32±2.1	10.1±2.6**	245.4±7.2	7
Uninjected control†	249.8±12.6	23.5±3.3	26.5±1.8	299.8±9.1	4
isl1 MO	214±13.4*	20.2±2.2	8.2±2.2**	242.4 ±14.0**	5
Control MO‡	170±4.6	16.3±2.0	22±2.0	208.3±6.6	4
sih MO	173±7.0	17.7±5.8	26.3±2.8	217±15.6	3
Uninjected control¶	243.7±26.5	28.7±1.3	32.3±4.1	304.7±22.6	3
fgf8 MO	153±5.5*	16.8±3.8*	25.8±2.3	195.5±5.9*	4
DMSO§	247±9.1	29.7±4.3	29.7±0.7	306.3±5.0	3
SU5402	246.4±10.8	6.2±2.0**	31±2.6	283.6±13.4	5

*Significant difference with control *P*<0.05.
**Significant difference with control *P*<0.01.
†Control for *Isl1* MO experiment.
‡Control for *sih* MO experiment.
¶Control for *fgf8* MO experiment.
§Control for SU5402 experiment.